Pulsed squeezed vacuum measurements without homodyning

Jérôme Wenger,[1] Jaromír Fiurášek,[2,3] Rosa Tualle-Brouri,[1] Nicolas J. Cerf,[2] and Philippe Grangier[1]

[1]*Laboratoire Charles Fabry de l'Institut d'Optique, CNRS UMR 8501, F-91403 Orsay, France*
[2]*QUIC, Ecole Polytechnique, CP 165, Université Libre de Bruxelles, 1050 Bruxelles, Belgium*
[3]*Department of Optics, Palacký University, 17. listopadu 50, 77200 Olomouc, Czech Republic*

Following a recent theoretical proposal [J. Fiurášek and N. J. Cerf, Phys. Rev. Lett. **93**, 063601 (2004)], we experimentally implement a scheme to measure the squeezing and purity of a single-mode squeezed vacuum state without an interferometric homodyne detection. The suggested setup is based on only a tunable beam splitter and a direct single-photon detector to fully characterize the generated Gaussian states. We discuss the experimental implementation of this procedure and compare it to other reference methods. A detailed exploitation of our results highlights some practical limitations of this method. This experimental work is followed by a detailed numerical analysis to derive the conditions required for the procedure to succeed. In particular, it is found that an overall single-photon detection efficiency of about 50% is needed, which is difficult to achieve in the present experiment.

I. INTRODUCTION

Squeezed states of light play an important role in the development of quantum information processing with continuous variables [1], where the information is encoded in two conjugate quadratures of an optical field mode. These states may, for example, be used as a main resource for quantum cryptographic protocols (see [2,3] and references therein). They may also serve as an entanglement source since combining two squeezed states at a beam splitter creates an entangled two-mode squeezed state such as those required for quantum teleportation [4] or dense coding [5]. In addition, squeezing has been shown to be an irreducible resource for realizing an arbitrary linear canonical transformation [6].

Any attempt to process squeezed states in quantum communication or computation systems will necessarily face the problem of characterizing these states. A possible complete description of a general quantum state is obtained by reconstructing its Wigner function using quantum tomographic procedures [7–9]. Alternatively, for a Gaussian state, which is fully described by its first- and second-order moments, another complete characterization is provided by the mean values of the conjugate quadratures x and p together with the associated covariance matrix γ. From this, one may compute various relevant parameters such as the maximum observable squeezing [10] or the degree of purity [11,12]. Finally, let us also mention that a lot of attention has been recently devoted to measurements of the photon statistics of quantum states [13–16].

In this paper, we follow an idea originally due to two of the present authors that consists of measuring the squeezing and purity of a Gaussian state without homodyne detection, that is, without any strong local oscillator beam providing a phase reference [17]. The suggested setup relies only on beam splitters and single-photon detectors. It generally requires a joint measurement of two copies of the Gaussian state, but single-copy measurements suffice if it is *a priori* known that the mean values of the quadratures vanish. Thus, in the latter case, which actually applies to all quantum in-

formation schemes based on squeezed vacuum states, no interferometric stability is required to determine the squeezing and purity, unlike with homodyne detection schemes.

Hereafter, we will focus on the important case of a single-mode squeezed vacuum state and discuss the experimental feasibility and relevance of this photon-counting characterization procedure. The experiment—carried out with state-of-the-art techniques—comes up with some practical limitations. For the rather generic states that we considered, the trace of the covariance matrix can be accurately determined by our setup, while the determinant of the covariance matrix (related to the state purity) requires a much higher overall single-photon detection efficiency. A detailed numerical analysis is then performed, showing that the present limitations might be overcome with an overall detection efficiency of about 50%. However, as discussed in the last section, this constraint appears to be rather difficult to meet in the present experiment.

Some useful notations to describe a squeezed vacuum beam are introduced in Sec. II. Section III then presents the experimental setup together with two classical and homodyne measurement procedures that are used as a reference to characterize the generated squeezed vacuum states. In Sec. IV, we briefly review the photon-counting characterization method applied to the special case of a single-mode Gaussian state (more details can be found in [17]). In Sec. V, we present the experimental results of this characterization method, while Sec. VI discusses the constraints on the global detection efficiency that are set by this method. Numerical simulations are used to illustrate the photon-counting method for values of the global detection efficiency that are presently unreachable with our standard experimental setup.

II. SQUEEZED VACUUM DESCRIPTION

Theoretically, a general Gaussian state with zero mean values of quadratures is fully characterized by its covariance matrix γ, which comprises the second moments of the con-
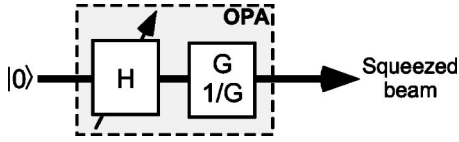
FIG. 1. General single-mode Gaussian state generation. H denotes the intensity gain of the phase-independent amplifier and G stands for the intensity gain of the phase-dependent amplifier.

jugate quadratures $x = a + a^\dagger$ and $p = (a - a^\dagger)/i$, with $[x,p] = 2i$. For states with zero mean values of quadratures, the covariance matrix γ can be expressed as follows:

$$\gamma = \begin{pmatrix} \langle x^2 \rangle & \frac{1}{2}\langle xp + px \rangle \\ \frac{1}{2}\langle xp + px \rangle & \langle p^2 \rangle \end{pmatrix}. \tag{1}$$

In order to determine the squeezing and purity, we need to measure only the two invariants of the covariance matrix, namely, the trace $\mathrm{Tr}(\gamma)$ and determinant $\det(\gamma)$.

From a more physical point of view, one can use the fact that the most general single-mode Gaussian state with $\langle x \rangle = \langle p \rangle = 0$ can be expressed as a squeezing operator applied to a Gaussian thermal state [12,19]. Translated into an optical setup, this is implemented by two simple linear amplifiers as depicted in Fig. 1: a *phase-insensitive* amplifier of gain H followed by a *phase-sensitive* amplifier of gains G and $1/G$ (in the following we take $G, H > 1$). In other words, the physics of the optical parametric amplifier (OPA) can be modeled by a "black box" squeezer which is parametrized by H and G. These two parameters are equivalent to the two phase-insensitive parameters $\mathrm{Tr}(\gamma)$ and $\det(\gamma)$ of the Gaussian state generated by the black box from the vacuum.

Let us describe the transformation effected by the amplifier depicted in Fig. 1. First, one can express the conjugate quadrature variables at the output of the OPA as

$$x_{\mathrm{out}} = \frac{1}{\sqrt{G}}(\sqrt{H}x_{\mathrm{vac}} + \sqrt{H-1}x_{\mathrm{anc}}), \tag{2}$$

$$p_{\mathrm{out}} = \sqrt{G}(\sqrt{H}p_{\mathrm{vac}} - \sqrt{H-1}p_{\mathrm{anc}}), \tag{3}$$

where we chose x_{out} (p_{out}) as the squeezed (antisqueezed) quadrature, and x_{vac} and x_{anc} denote the vacuum and ancilla quadratures at the input ports of the total amplifier, respectively. One can then express the variances of the squeezed and antisqueezed quadratures at the output of the OPA as

$$V_{\mathrm{min}} = (2H-1)/G, \tag{4}$$

$$V_{\mathrm{max}} = (2H-1)G. \tag{5}$$

The trace and determinant of the covariance matrix read

$$\mathrm{Tr}(\gamma) = V_{\mathrm{min}} + V_{\mathrm{max}}, \tag{6}$$

$$\det(\gamma) = V_{\mathrm{min}}V_{\mathrm{max}}. \tag{7}$$

This system of equations can be inverted, and the squeezed and antisqueezed variances can be expressed in terms of the trace and the determinant of γ,
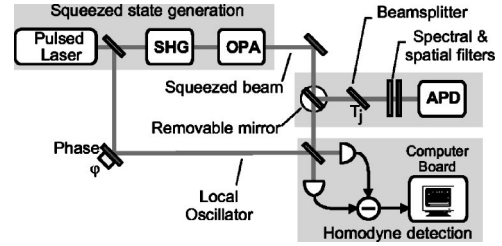

FIG. 2. Simplified experimental setup. SHG, second harmonic generation module; OPA, degenerate optical parametric amplifier; APD, avalanche photodiode photon-counting module.

$$V_{\mathrm{max,min}} = \frac{1}{2}[\mathrm{Tr}(\gamma) \pm \sqrt{\mathrm{Tr}^2(\gamma) - 4\det(\gamma)}]. \tag{8}$$

Finally, the purity $\mathcal{P} = \mathrm{Tr}[\rho^2]$ of a mixed state ρ is, for any single-mode Gaussian state, directly linked to the average photon number of thermal noise $\bar{n} = H - 1$:

$$\mathcal{P} = \frac{1}{2\bar{n}+1} = \frac{1}{2H-1}. \tag{9}$$

Equivalently, in terms of the covariance matrix, we have

$$\mathcal{P} = \frac{1}{\sqrt{\det(\gamma)}}. \tag{10}$$

III. REFERENCE CLASSICAL AND HOMODYNE CHARACTERIZATION METHODS

A different scheme for pulsed squeezed light generation has recently been developed [18] and will be used here to compare the photon-counting characterization method to standard methods. The experimental setup is depicted in Fig. 2. The initial pulses are obtained from a titanium-sapphire laser delivering nearly Fourier-transform-limited pulses centered on 846 nm, with a duration of 150 fs, a typical energy of 40 nJ, and a repetition rate of 780.4 kHz. These pulses are frequency doubled in a single pass through a thin (100 μm) crystal of potassium niobate ($KNbO_3$), cut and temperature-tuned for noncritical type-I phase matching. The second harmonic power is large enough to obtain a significant single-pass parametric gain in a similar $KNbO_3$ crystal used in a type-I spatially degenerate configuration.

The squeezed beam can then be directed onto two different detection modules using a removable mirror.

(i) Homodyne detection module: the squeezed vacuum beam interferes with the local oscillator beam in a balanced homodyne detection setup. A main feature of our experiment is that all the processing is done in the time domain, not in the frequency domain. For each incoming pulse, the fast acquisition board samples one value of the signal quadrature in phase with the local oscillator [18].

(ii) Photon counting module: the squeezed vacuum beam is transmitted via a beam splitter of tunable transmittance T and then passes through a spatial filter (made of two Fourier-conjugated pinholes) and a 3 nm spectral filter centered at the laser wavelength, before being detected by a silicon avalanche photodiode (APD).

To start the characterization procedure, a basic measurement is to monitor the classical amplification and deamplification of a probe taken from the fundamental beam. This is easily done by direct detection of a probe beam averaged power on a photodiode. Setting the relative phase between the probe and the second harmonic pump beam allows us to tune the classical gain from the minimum deamplification intensity gain $\mathcal{G}_{\min}$ to the maximum gain $\mathcal{G}_{\max}$. The measurement of the classical gains $\mathcal{G}_{\min}$ and $\mathcal{G}_{\max}$ gives an estimate of G and H,

$$G = \sqrt{\mathcal{G}_{\max}/\mathcal{G}_{\min}}, \tag{11}$$

$$H = \sqrt{\mathcal{G}_{\max}\mathcal{G}_{\min}}. \tag{12}$$

The experimental results of the squeezed vacuum characterization for different values of the pump power are shown in Figs. 3 and 4, marked as "Classical" (black disks).

Following the principle of quantum tomography, a powerful approach is to completely characterize the squeezed vacuum by conjugate quadratures homodyne measurements. The time-resolved balanced homodyne detection allows us to measure the squeezed and antisqueezed quadrature variances $V_{\mathrm{hom,min}}$ and $V_{\mathrm{hom,max}}$. Imperfections and losses in this detection are modeled by a beam splitter of transmission η_{hom} (in intensity). The procedure to measure the detection efficiency is well established from squeezing experiments [20], and it can be cross-checked by comparing the classical parametric gain and the measured degree of squeezing. We note the homodyne detection efficiency $\eta_{\mathrm{hom}}= \eta_T \eta_H^2 \eta_D = 0.76 \pm 0.01$, where the overall transmission $\eta_T = 0.92$, the mode-matching visibility $\eta_H = 0.935$, and the detector efficiency $\eta_D = 0.945$ are independently measured. Given this efficiency, one can correct for losses and deduce the squeezed and antisqueezed quadrature variances at the output port of the OPA, namely,

$$V_{\min} = (V_{\mathrm{hom,min}} - 1 + \eta_{\mathrm{hom}})/\eta_{\mathrm{hom}}, \tag{13}$$

$$V_{\max} = (V_{\mathrm{hom,max}} - 1 + \eta_{\mathrm{hom}})/\eta_{\mathrm{hom}}. \tag{14}$$

This allows the full characterization of the state parameters $[\mathrm{Tr}(\gamma), \det(\gamma)]$ or the OPA parameters (G,H) following the above formulas. The experimental results of this second characterization method are also displayed in Figs. 3 and 4, marked as "Homodyne" (gray squares). As one can notice in Figs. 3 and 4, for high pump powers the "homodyne" and "classical" values do not well overlap within their respective error bars. A main reason for this is that the "black-box" model developed above is basically a *single-mode* model, and thus suffers from fundamental limitations, while for high pump powers the physics involved in parametric deamplification is known to fall into a multimode regime [21].

In the following, we will use these "classical" and "homodyne" methods as references to check the validity of the photon-counting characterization.

IV. PHOTON-COUNTING CHARACTERIZATION METHOD

Let us briefly introduce the methods implemented here for measuring the properties of a Gaussian state by photon
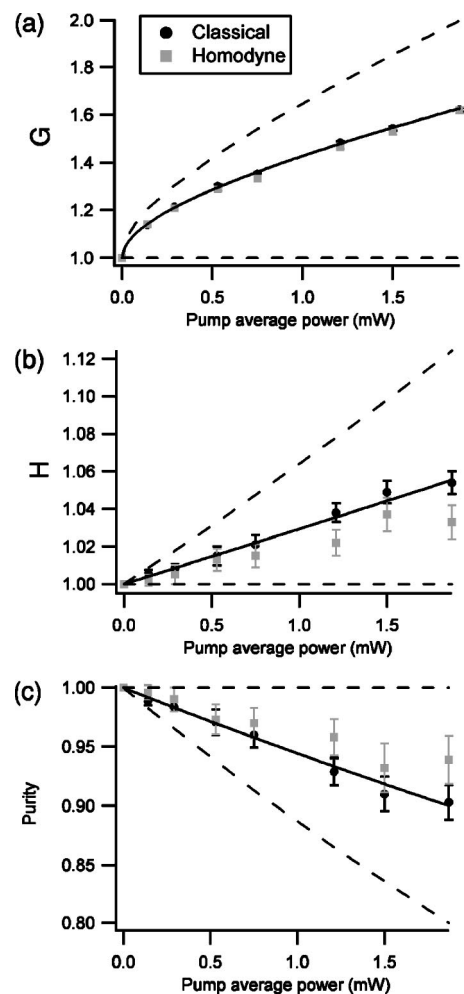

FIG. 3. Parametric gains G, H, and purity $\mathcal{P}$ versus average pump power at 423 nm. The solid line corresponds to a fit on the classical results according to plane wave theory. "Classical" stands for the classical probe gain measurements (black disks); "Homodyne" stands for the balanced homodyne detection variance measurements (gray squares). The bounds inferred from the photon-counting method, to be described in Sec. IV, are indicated by the two dashed lines (see further explanations in Sec. V).

counting, which are derived from the original procedure presented in [17]. We will restrict our attention to a single-mode Gaussian state with zero coherent displacement, $\langle x \rangle = \langle p \rangle = 0$, which is the case in the present experiment depicted in Fig. 2. The squeezed vacuum mode impinges on a beam splitter with tunable transmittance T before being measured by an avalanche photodiode that is sensitive to single photons and can respond with two measurement outcomes, either a click or a no-click. This detector with overall detection efficiency η_{APD} can be modeled as a beam splitter with transmittance η_{APD} followed by an ideal detector that performs a dichotomic measurement described by the projectors $\Pi_0 = |0\rangle\langle 0|$ (a no-click) and $\Pi_1 = \mathbb{1} - \Pi_0$ (a click). In the rest of this section, we assume that the detector is ideal, while $\eta_{\mathrm{APD}} \neq 1$ can be taken into account by substituting $T \to \eta_{\mathrm{APD}} T$.

The probability of no-click of an ideal detector is given by $P = \langle 0 | \rho | 0 \rangle$. It can be determined from the Husimi Q function which provides a phase-space representation of the state
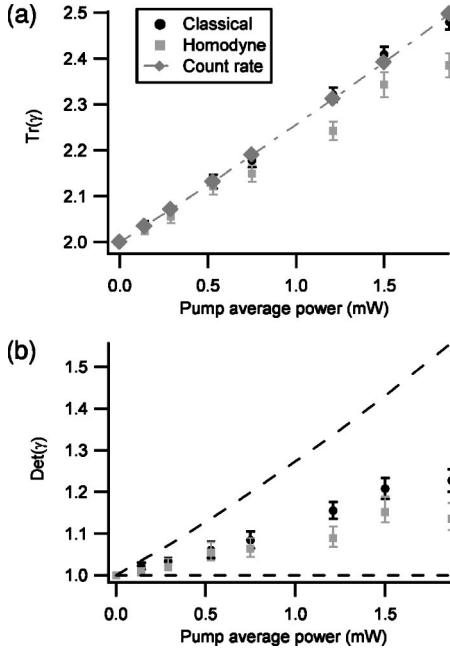
FIG. 4. Trace $\text{Tr}(\gamma)$ and determinant $\det(\gamma)$ versus average pump power at 423 nm. The annotations are the same as in Fig. 3. For ease of viewing, the trace values obtained from the photon-counting method (gray diamonds) are linked by a dash-dotted line in (a). In (b), the two dashed lines indicate the limits on the determinant knowledge obtained from the photon-counting method (see further details in Sec. V).

ρ: $Q(\alpha)$ is defined as the overlap of ρ with a coherent state $|\alpha\rangle$. The Q function of a Gaussian state with zero mean values of quadratures is a Gaussian function centered at the origin,

$$Q(r) = \frac{1}{2\pi\sqrt{\det(\gamma+I)}} \exp\left(-\frac{1}{2}r^T(\gamma+I)^{-1}r\right), \quad (15)$$

where $r=(x,p)$ and I is the identity matrix. Since the vacuum is just a special case of a coherent state, the probability of projecting the state (15) onto vacuum reads $P=4\pi Q(0)$ and, on inserting $r=0$ in Eq. (15), we obtain

$$P = \frac{2}{\sqrt{\det(\gamma+I)}}. \quad (16)$$

The characterization method works by carrying out measurements of the probabilities of no-click P_j for several different transmittances T_j. The covariance matrix γ_j of the state after passing through the beam splitter reads $\gamma_j = T_j\gamma + (1-T_j)I$, where γ is the covariance matrix of the input state. On inserting γ_j into Eq. (16), we obtain after some simple algebra

$$\frac{4}{P_j^2} = T_j^2 \det(\gamma) + T_j(2-T_j)\text{Tr}(\gamma) + (2-T_j)^2. \quad (17)$$

We thus find that P_j depends on T_j (or, more generally, on $\eta_{\text{APD}}T_j$) and on the determinant and trace of the covariance matrix γ of the input state. Note that $4/P_j^2$ is a *linear* function of the two unknown quantities $\det(\gamma)$ and $\text{Tr}(\gamma)$. Thus,

measurements of P_j for only two different transmittances simply suffice to determine the trace and the determinant, as the system of linear equations (17) can easily be solved and yields

$$\text{Tr}(\gamma) = \frac{2}{T_2 - T_1}\left(\frac{T_2}{T_1 P_1^2} - \frac{T_1}{T_2 P_2^2}\right) + 2 - \frac{2}{T_1} - \frac{2}{T_2}, \quad (18)$$

$$\det(\gamma) = \frac{2}{T_1 - T_2}\left(\frac{2-T_2}{T_1 P_1^2} - \frac{2-T_1}{T_2 P_2^2}\right) + \frac{(2-T_1)(2-T_2)}{T_1 T_2}. \quad (19)$$

Then, having obtained the determinant and trace of γ, we can determine the squeezing properties of the state from Eq. (8) as well as its purity (10).

Dealing with a real world experiment, with unavoidable noises and uncertainties, a more realistic procedure would consist in performing the experiment for as many transmission values T_j as possible and then trying to get the most information from these various measurements. One possibility to gain information from more than two measurements is to implement a maximum-likelihood (ML) parameter estimation method (for a review, see, for instance, Refs. [22–24]). This procedure provides the values of the parameters $\text{Tr}(\gamma)$ and $\det(\gamma)$ that are the most likely to yield the observed experimental data. In mathematical terms, this boils down to finding the maximum of the joint probability density

$$\mathcal{L}(\text{Tr}(\gamma), \det(\gamma)) = \prod_{j=1}^{n} P_j^{N_{\text{rep}} - C_j}(1 - P_j)^{C_j}, \quad (20)$$

which is called the likelihood function of the given experimental data. Here, C_j denotes the number of photodetector clicks per second for transmittance T_j and N_{rep} is the pulse repetition rate. The probability P_j is linked to $\text{Tr}(\gamma), \det(\gamma)$, and T_j by Eq. (17). Actually, we also have to take into account some additional constraints on the parameters $\text{Tr}(\gamma)$ and $\det(\gamma)$. The fact that the covariance matrix γ is positive definite and must satisfy the generalized Heisenberg uncertainty relation $\det(\gamma) \geq 1$ sets the constraints

$$1 \leq \det(\gamma) \leq \left(\frac{\text{Tr}(\gamma)}{2}\right)^2. \quad (21)$$

The next section now presents and discusses the results of this characterization procedure from its experimental implementation.

V. EXPERIMENTAL RESULTS

Hereafter, we denote by T only the transmittance of the (lossless) variable beams plitter. Nonunit transmissions of the spectral and spatial filters and imperfect detection efficiency are taken into account by the overall efficiency parameter η_{APD} of the APD detection.

A first step is to estimate this overall efficiency η_{APD} in order to apply the characterization method. Setting the supplementary beam splitter to a transmittance of 1, η_{APD} can be estimated from the measurement of the number of
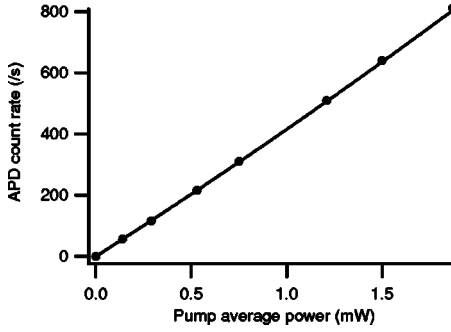
FIG. 5. Number of photon-detection events per second versus average pump power for maximum transmission of the variable beam splitter $T=1$. The solid line is a fit following Eq. (22), from which we extracted an estimate of the photon-counting detector efficiency $\eta_{APD}=0.84\times10^{-2}\pm0.013\times10^{-2}$.

photon-counting events detected per second, N_{clicks}, for different pump powers. In the limit of low η_{APD}'s, the number of clicks detected per second can be approximated as

$$N_{clicks} = \frac{1}{2}\eta_{APD}N_{rep}[(H-1/2)(G+1/G)-1], \quad (22)$$

where the dependence of G and H versus the pump power is obtained from the curve fit on the "classical" results presented in Figs. 3(a) and 3(b), while $N_{rep}=780.4$ kHz is the repetition rate. With our experimental results (see Fig. 5) the fit of N_{clicks} versus the pump power gives $\eta_{APD}=0.84\times10^{-2}\pm0.013\times10^{-2}$. This value can be cross-checked with the overall efficiency inferred from transmission factors of an intense probe beam: the spatial and spectral filters transmit, respectively, 16% and 17% of the probe beam, while the APD quantum efficiency is estimated to about 50%, leading to an overall detection efficiency of the probe of about 1.4%. The difference between the latter value and the above estimate of η_{APD} may be explained by slight differences between the modes of the probe (set for maximal classical deamplification) and the squeezed vacuum.

In our experiment, we used between four and six different settings for the beam splitter transmittance T_j. For each T_j, we performed 100 measurements of the number of clicks per second to get a good statistical accuracy on C_j. As a result of an appropriate gating of the detection, the dark count rate remained reasonably low (about 20 s^{-1}) and was subtracted from the data.

As shown above, only two different settings of the beam splitter transmittance, T_1 and T_2, are enough to extract the value of $\det(\gamma)$ and $\mathrm{Tr}(\gamma)$ following Eqs. (18) and (19). Actually, formula (18) indeed leads to an estimate of $\mathrm{Tr}(\gamma)$ which is satisfactorily close to the values obtained from either homodyne or classical measurement. However, as far as the determination of $\det(\gamma)$ is concerned, the formula (19) does not give any reliable estimate. This results from the fact that, in the experiment, we have to work with small detection efficiencies $\eta_{APD}\ll1$ so that small uncertainties on P_1,P_2,T_1,T_2 have much larger influence on $\det(\gamma)$ than on $\mathrm{Tr}(\gamma)$. For instance, if we take the derivative of $\mathrm{Tr}(\gamma)$ and $\det(\gamma)$ with respect to P_1, we find

$$\frac{d\,\mathrm{Tr}(\gamma)}{dP_1} = \frac{4}{\eta_{APD}P_1^3}, \quad (23)$$

$$\frac{d\,\det(\gamma)}{dP_1} = \frac{-16}{\eta_{APD}^2 P_1^3}. \quad (24)$$

This shows that in our experimental setup the determinant is about 400 times more sensitive to small uncertainties on P_1 than the trace.

In order to gain information on the determinant of the covariance matrix as well as to increase the accuracy of the estimate of its trace, we used the full set of measurements for the different beam splitter transmittances by performing a maximum-likelihood estimation as introduced in the previous section. The logarithm of the likelihood function $\mathcal{L}$ given by Eq. (20) was computed from the measured data, the above estimate of the overall detection efficiency η_{APD}, and the values of the transmittance T_j obtained from direct power transmission of the probe beam. The global maximum of $\log(\mathcal{L})$ was then found by a brute force numerical search. The experimental results of the estimated $\mathrm{Tr}(\gamma)$ for several different pump powers are shown in Fig. 4(a), and fully coincide with the values inferred from the classical gain measurements. Out of the three trace-estimation procedures, the photon-counting method associated with log-likelihood maximization provides the lowest uncertainty on the result.

Unfortunately, given the low detection efficiency η_{APD} of our experimental setup, the likelihood function is almost flat as a function of $\det(\gamma)$ in the region that is allowed by the constraints (21). Consequently, no reliable estimate of the determinant could be obtained from our experimental data, the log-likelihood maximization method returning essentially a random value between 1 and $[\mathrm{Tr}(\gamma)/2]^2$. Similarly, our experimental data provide bounds on only the parametric gains G and H given the sole knowledge of the trace $\mathrm{Tr}(\gamma)$:

$$1 \leq G \leq \left(\frac{\mathrm{Tr}(\gamma)+\sqrt{\mathrm{Tr}(\gamma)^2-4}}{\mathrm{Tr}(\gamma)-\sqrt{\mathrm{Tr}(\gamma)^2-4}}\right)^{1/2}, \quad (25)$$

$$1 \leq H \leq \frac{\mathrm{Tr}(\gamma)+2}{4}. \quad (26)$$

Thus, the dashed lines in Figs. 3(a), 3(b), 3(c), and 4(b) take into account the fact that no estimate of the determinant better than the bounds (21) could be obtained by the photon-counting method given the estimate of the trace. We also tried various other numerical methods—such as least–squares inversion—but none provided a reliable estimate of $\det(\gamma)$.

Some better insight into the intrinsic difficulty of getting an estimate of $\det(\gamma)$ can be obtained by rewriting Eq. (17) as

$$\frac{4}{P_j^2} = [\det(\gamma)-\mathrm{Tr}(\gamma)+1]\eta_{APD}^2 T_j^2 + 2[\mathrm{Tr}(\gamma)-2]\eta_{APD}T_j + 4. \quad (27)$$

It becomes clear that the determinant is linked to the second-order dependence of P_j^{-2} in the transmittance, while the trace

can be directly obtained from the linear dependence of P_j^{-2}. The basic difficulty of estimating $\det(\gamma)$ results from the fact that the relevant information is hidden in terms of order $(\eta_{APD}T)^2$, which are very small for our experimental data given the low values of η_{APD}.

One could then try to increase the overall APD detection efficiency η_{APD} by releasing either the spatial or spectral filtering conditions. However, from an experimental point of view, this does not seem realistic for several reasons.

First, we would move to a region where the physics becomes multimode, which is clearly outside the framework of the developed model. In principle, the photon-counting method allows one to check whether the single-mode description of the experiment is appropriate or not. If only a single mode is detected, then P^{-2} should be a quadratic polynomial in $\eta_{APD}T$ [cf. Eq. (27)]. More generally, if the detector effectively registers light from N modes in a Gaussian state, then P^{-2} becomes a polynomial of $2N$th order in $\eta_{APD}T$ [17]. So after measuring P as a function of $\eta_{APD}T$ one could perform a fitting to determine the minimal number of modes N that is necessary for the description of the observed signal. However, a successful application of this technique would require a very high precision in the measurement of P and a high η_{APD}.

A second problem with removing the spatial and/or spectral filters is that we would lose any possibility of cross-checking our results with classical parametric gain or homodyne measurements. Last, even in the case of no spatial filter and 10 nm spectral filter, the overall APD detection efficiency will remain low given our experimental setup, and we do not expect to gain much according to our numerical simulations of the constraints on the global efficiency presented below.

VI. NUMERICAL SIMULATIONS

We have seen that the low APD detection efficiency η_{APD} precludes a reliable estimate of $\det(\gamma)$ via the photon-counting method. It is thus important to determine the efficiency η_{APD} that should be attained in order to be able to estimate $\det(\gamma)$ with acceptably small errors. More generally, it is interesting to investigate the dependence of the estimation errors on η_{APD}. For this purpose, we have carried out extensive numerical simulations of the experiment for several values of η_{APD}, the other parameters of the simulation being chosen in accordance with the experimental values. In particular, we have assumed a measurement repetition rate $N_{rep}=780.4$ kHz and a total measurement time $t=100$ s for each transmittance T_j. The total number of measurements for each T_j is then given by $N_{tot}=N_{rep}t$. We have further assumed that measurements were carried out for four different transmittances $T_1=1$, $T_2=0.75$, $T_3=0.5$, and $T_4=0.25$, and we used the experimentally obtained values $\det(\gamma)=1.156$ and $\mathrm{Tr}(\gamma)=2.321$ as a typical example (corresponding to a pump average power of 1.21 mW).

The determinant and the trace of γ were estimated from the simulated experimental data with the help of the maximum-likelihood technique described in the preceding section. Since the ML estimator is generally biased, we de-
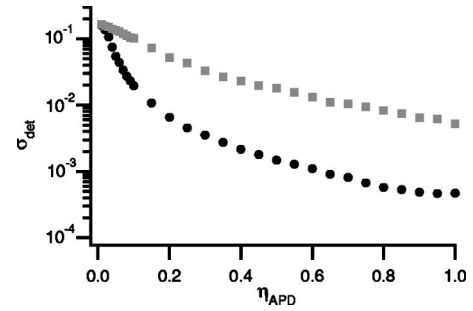

FIG. 6. The dependence of the variance σ_{det} of the estimation of $\det(\gamma)$ on the detector efficiency η_{APD} in cases when the parameters T_j and η_{APD} are known exactly (circles) and when the experimental uncertainties of T_j are 0.5% and the relative uncertainty of η_{APD} is 1% (squares). See text for further details.

fine the deviation of the estimate from the true value as

$$\sigma_{det}^2 = \langle [\det(\gamma)_{est} - \det(\gamma)_{true}]^2 \rangle,$$

$$\sigma_{Tr}^2 = \langle [\mathrm{Tr}(\gamma)_{est} - \mathrm{Tr}(\gamma)_{true}]^2 \rangle, \tag{28}$$

where $\langle \rangle$ indicates averaging over an ensemble of experiments. In practice, we simulated 1000 times the whole experiment, from data acquisition to ML estimation, and we then calculated Eq. (28) by averaging over the ensemble. Since the total number of measurements N_{tot} was very large, we approximated the binomial distribution of C_j by a normal distribution with the same mean and variance.

In addition to the statistical fluctuations of C_j and the intrinsic difficulty of estimating $\det(\gamma)$ at low detection efficiencies, other factors contribute to the estimation errors, namely, the uncertainty in the knowledge of T_j and η_{APD}. To isolate the errors stemming from low η_{APD}, we have first assumed that all parameters T_j and η_{APD} are known precisely; hence the statistical fluctuations of C_j are the only source of errors. The resulting σ_{det} is plotted as circles in Fig. 6. For very low η_{APD}, the estimates of $\det(\gamma)$ are randomly distributed in the interval $[1,[\mathrm{Tr}(\gamma)]^2/4]$ and $\sigma_{det} \approx \frac{1}{2}[\mathrm{Tr}^2(\gamma)/4-1]$. The estimation error rapidly decreases as η_{APD} grows, and our numerical simulations reveal that a reliable estimate of $\det(\gamma)$ with $\sigma_{det}<10^{-2}$ could be obtained for $\eta_{APD}>15\%$.

The uncertainties of T_j and η_{APD} significantly increase the estimation error for higher η_{APD}. We have performed numerical simulations taking into account that T_j's are known with an uncertainty of 0.5%, and the relative uncertainty of η_{APD} is 1%, which corresponds to the actual experimental situation. The resulting σ_{det} is plotted as squares in Fig. 6. We observe that σ_{det} is much higher than in the previous case, except for the region of very small η_{APD}. To obtain a satisfactorily accurate estimate of $\det(\gamma)$ with $\sigma \approx 2 \times 10^{-2}$, we need $\eta_{APD} \gtrsim 50\%$.

In order to demonstrate that $\eta_{APD}=50\%$ is indeed sufficient for the whole range of values of the pump power, we have simulated the results of an experiment at $\eta_{APD}=50\%$ for the same values of the pump power as in Figs. 3 and 4. The results are given in Fig. 7 which shows the mean estimated values of $\det(\gamma)$ as well as the resulting error bars. We
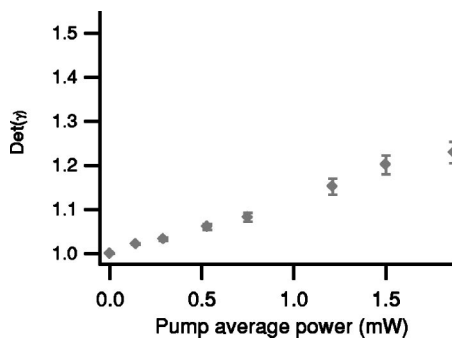
FIG. 7. Results of the estimation of $\det(\gamma)$ from simulated photon-counting measurement assuming overall detection efficiency $\eta_{APD}=50\%$. This figure has been scaled so as to be easily compared to the experimental results presented on Fig. 4(b).

find that these estimates are in very good agreement with the true values used in the simulation.

Finally, note that our numerical simulations also confirm that the estimate of $\text{Tr}(\gamma)$ is very accurate: we have found that $\sigma_{\text{Tr}} \lesssim 10^{-2}$ even for η_{APD} as low as 1%.

VII. CONCLUSIONS

In this paper, we have discussed the experimental implementation of a direct photon counting method to fully characterize squeezed vacuum states. In contrast to homodyning, this method does not require any interferometric detection to evaluate the squeezing and purity of the squeezed vacuum state. For the rather generic states that we considered, the trace of the covariance matrix can be accurately determined, even with an overall detection efficiency η in the percent range, while its determinant (related to the state purity) requires a much higher η, typically around 50%.

In principle, such efficiencies are well within the reach of silicon photon-counting avalanche photodiodes, but an important problem remains: most sources do not emit single-mode Gaussian light, but rather multimode light. This is not a problem when a homodyne detection is used, because the local oscillator acts as a very efficient single-mode filter. On the other hand, a photon counter detects photons in any mode. Therefore, detecting a good approximation of a single-mode state requires appropriate spatial and spectral filters, respectively obtained from pinholes and diffraction gratings.

Unless a special effort is made, these filters will have a low overall transmission (a few percent in our experiment), and thus the direct detection method will fail to determine the state purity. In principle, there are various ways for improvement, which are open for further experimental work. Ideally, the source itself should emit single-mode light, which might be obtained by appropriate phase-matching conditions in a $\chi^{(2)}$ nonlinear crystal. On the filtering side, interferometric multidielectric filters provide transmission values which are much higher than those of standard slits and grating setups. A combination of these various techniques will be probably needed to reach the high overall efficiencies needed for many potential applications.

As a conclusion, it appears that a broad variety of techniques is proposed to characterize quantum continuous variables, and that these methods will certainly continue to develop for applications in quantum cryptography, quantum communications, and possibly quantum computing. Perhaps the most appealing application of the photon-counting method is the direct determination of the entanglement of two-mode Gaussian states by measuring only the purity of the two-mode state and the marginal purities of the single-mode states on each side [17,25]. All these purities can be determined with the photon-counting method using only local measurements. The distinct feature of this approach is that no interferometric stability is required if one is dealing with squeezed vacuum states, which is the case in many experiments. This may be an important advantage in the characterization of entanglement distribution over long-distance continuous-variable quantum communication networks.

[1] S. L. Braunstein and A. K. Pati, *Quantum Information with Continuous Variables* (Kluwer Academic, Dordrecht, 2003).

[2] N. J. Cerf, M. Lévy, and G. Van Assche, Phys. Rev. A **63**, 052311 (2001).

[3] F. Grosshans and P. Grangier, Phys. Rev. Lett. **88**, 057902 (2002); F. Grosshans, G. Van Assche, J. Wenger, R. Brouri, N. J. Cerf, and Ph. Grangier, Nature (London) **421**, 238 (2003).

[4] C. H. Bennett *et al.*, Phys. Rev. Lett. **70**, 1895 (1993); S. L. Braunstein and H. J. Kimble, *ibid.* **80**, 869 (1998); A. Furusawa *et al.*, Science **282**, 706 (1998).

[5] S. L. Braunstein and H. J. Kimble, Phys. Rev. A **61**, 042302 (2000).

[6] S. L. Braunstein, e-print quant-ph/9904002.

[7] U. Leonhardt, *Measuring the Quantum State of Light* (Cambridge University Press, Cambridge, 1997).

[8] G. Breitenbach, S. Schiller, and J. Mlynek, Nature (London) **387**, 471 (1997).

[9] D.-G. Welsch, W. Vogel, and T. Opatrný, *Homodyne Detection and Quantum-State Reconstruction*, Progress in Optics, Vol. 39, edited by E. Wolf (Elsevier, Amsterdam, 1999).

[10] R. Simon, N. Mukunda, and B. Dutta, Phys. Rev. A **49**, 1567 (1994).

[11] M. S. Kim, J. Lee, and W. J. Munro, Phys. Rev. A **66**, 030301 (2002).

[12] M. G. A. Paris, F. Illuminati, A. Serafini, and S. De Siena, Phys. Rev. A **68**, 012314 (2003).

[13] D. Mogilevtsev, Opt. Commun. **156**, 307 (1998); A. R. Rossi, S. Olivares, and M. G. A. Paris, e-print quant-ph/0405139.

[14] E. Waks, E. Diamanti, B. C. Sanders, S. D. Bartlett, and Y. Yamamoto, Phys. Rev. Lett. **92**, 113602 (2004).

[15] J. Rehacek, Z. Hradil, O. Haderka, J. Perina, Jr., and M. Hamar, Phys. Rev. A **67**, 061801 (2003); O. Haderka, M. Hamar, and J. Perina, Eur. Phys. J. D **28**, 149 (2004).

[16] D. Achilles *et al.*, J. Mod. Opt. **51**, 1499 (2004).

[17] J. Fiurášek and N. J. Cerf, Phys. Rev. Lett. **93**, 063601 (2004).

[18] J. Wenger, R. Tualle-Brouri, and P. Grangier, Opt. Lett. **29**, 1267 (2004) See also e-print quant-ph/0402192.

[19] G. Adam, J. Mod. Opt. **42**, 1311 (1995).

[20] R. E. Slusher, P. Grangier, A. LaPorta, B. Yurke, and M. J. Potasek, Phys. Rev. Lett. **59**, 2566 (1987).

[21] A. LaPorta and R. E. Slusher, Phys. Rev. A **44**, 2013 (1991).

[22] Z. Hradil, Phys. Rev. A **55**, R1561 (1997).

[23] G.M. D'Ariano, M. G.A. Paris, and M. F. Sacchi, Phys. Rev. A **62**, 023815 (2000).

[24] J. Řeháček, Z. Hradil, and M. Ježek, Phys. Rev. A **63**, 040303 (2001).

[25] G. Adesso, A. Serafini, and F. Illuminati, Phys. Rev. Lett. **92**, 087901 (2004).